Molecular Crystals and Liquid Crystals

Publication details, including instructions for authors and subscription information:
http://www.tandfonline.com/loi/gmcl20

A BIFURCATION STUDY OF WAVE PATTERNS FOR ELECTROCONVECTION IN NEMATIC LIQUID CRYSTALS

Gerhard Dangelmayr [a] & Iuliana Oprea [a]

[a] Department of Mathematics, Colorado State University, Ft. Collins, CO, 80523, USA

Version of record first published: 07 Jan 2010

To cite this article: Gerhard Dangelmayr & Iuliana Oprea (2004): A BIFURCATION STUDY OF WAVE PATTERNS FOR ELECTROCONVECTION IN NEMATIC LIQUID CRYSTALS, Molecular Crystals and Liquid Crystals, 413:1, 305-320

To link to this article: http://dx.doi.org/10.1080/15421400490437051

Mol. Cryst. Liq. Cryst., Vol. 413, pp. 305/[2441]–320/[2456], 2004

ISSN: 1542-1406 print/1563-5287 online
DOI: 10.1080/15421400490437051

Taylor & Francis
Taylor & Francis Group

A BIFURCATION STUDY OF WAVE PATTERNS FOR ELECTROCONVECTION IN NEMATIC LIQUID CRYSTALS

Gerhard Dangelmayr and Iuliana Oprea
Department of Mathematics, Colorado State University, Ft. Collins, CO 80523, USA

We present the results of a bifurcation analysis of electroconvection in a planar layer of nematic liquid crystals, based on the recently introduced weak electrolyte model, which is an extension of the standard model to an electrodiffusion model with two active ion species. We show numerically that in certain regions of the space of material parameters a primary instability involving four oblique traveling rolls can occur. Near threshold the model equations are reduced to a system of normal form ODEs that admits six distinct basic wave patterns, and allows to classify the stability of these waves in terms of five nonlinear coefficients. For parameters matched to 152 and MBBA I, the stable wave patterns are traveling rolls and alternating waves. Approaches towards a refined stability analysis based on an extension of the ODE normal form to a system of globally coupled Ginzburg Landau equations are briefly discussed.

Keywords: electroconvection; Ginzburg-Landau equations; nematic; wave patterns

1. INTRODUCTION

Electroconvection in nematic liquid crystals (NLC) is a paradigm for pattern formation in anisotropic systems, exhibiting a rich variety of dynamical structures [1,2]. NLC differ from isotropic fluids since they exhibit long range microscopic molecular alignment, that leads to anisotropic macroscopic properties. When an electric potential is applied across a thin NLC layer confined between two electrode plates, an electrohydrodynamic instability can occur above a critical field strength [1]. The traditionally used mathematical model to describe this type of instability is the so-called standard model (SM) [3–6], where the charge conduction in the liquid crystal is assumed ohmic. The SM involves equations for the velocity field, the

Address correspondence to Gerhard Dangelmayr, Department of Mathematics, Colorado State University, Ft. Collins, CO 80523, USA.

director, the electric potential and charge derived from the generalized Navier-Stokes equations for an anisotropic electrically conducting fluid, the conservation of charge, and Poisson's and Ohm's laws. The SM explains quantitatively the phenomena observed in the conduction range, as well as several secondary instabilities observed experimentally such as the transition to zig-zag rolls, stationary and oscillatory bimodal patterns, and abnormal rolls [7], but it cannot predict states like traveling waves.

The recently introduced weak electrolyte model (WEM) of Kramer and Treiber [8–10] incorporates into SM ionic migration, molecular dissociation-recombination reactions and their effects on the conductivity, and provides a basis for the understanding of the Hopf bifurcation observed quite frequently at threshold [11–13]. In the WEM the ohmic conductivity is replaced by two dynamically active species of charge carriers, one positive and one negative. The constant ohmic conductivity of SM becomes a dynamical variable on its own with Ohm's law replaced by migration and diffusion parts of the current. The additional effects can lead to a distinctive change of the threshold behavior of the electroconvective instability, namely to traveling patterns instead of static ones, and therefore may predict Hopf bifurcation and explain the experimentally observed phenomena. In addition the WEM predicts a subcritical bifurcation for stationary rolls in the vicinity of the crossover to the Hopf bifurcation.

In this work we present results of a weakly nonlinear bifurcation analysis of the weak electrolyte model in the limit of zero momentum diffusion and zero charge relaxation times. Our main purpose is to demonstrate the existence of a Hopf-type primary instability involving four oblique rolls, and to analyze the resulting convective wave patterns predicted by this instability beyond threshold. In Section 2 we introduce the basic model equations, and in Section 3 we present results of our bifurcation study. The numerical approach for computing critical values and nonlinear coefficients is based on a $3N$-mode approximation combined with an analytically exact solution of the linearized velocity equations. In Section 4 we briefly discuss Ginzburg Landau extensions of our normal form and give an outlook on future work.

2. BASIC EQUATIONS

The continuum theory of Ericksen [14] and Leslie [15] treats NLC as incompressible fluids in which the average molecular axis is described locally by a director field $\mathbf{n}$ of unit vectors. Assuming a layer of NLC sandwiched between two horizontal plates, the Leslie-Erickson equations for $\mathbf{n}$ and the generalized Navier Stokes equations for the fluid velocity $\mathbf{v}$ and the

pressure p in the presence of an electric field $\mathbf{E}$ are

$$(\partial_t + \mathrm{v}\cdot\nabla)\mathbf{n} = \omega\times\mathbf{n} + \mathbf{d}(\lambda\mathbf{A}\mathbf{n} - \mathbf{h}), \tag{1}$$

$$P_2(\partial_t + \mathrm{v}\cdot\nabla)\mathbf{v} = -\nabla\mathbf{p} - \nabla\cdot(\mathbf{T}+\Pi) + \pi^2\rho\mathbf{E}, \tag{2}$$

$$\nabla\cdot\mathbf{v} = 0. \tag{3}$$

Here $\omega = \frac{1}{2}(\nabla\times\mathbf{v})$ is the vorticity, and the molecular field $\mathbf{h}$ is given by

$$\mathbf{h} = 2\left(\frac{\partial f}{\partial\mathbf{n}} - \nabla\cdot\frac{\partial f}{\partial\nabla\mathbf{n}}\right) - \varepsilon_a\pi^2(\mathbf{n}\cdot\mathbf{E})\mathbf{E},$$

which involves the elastic energy density

$$2f = (\nabla\cdot\mathbf{n})^2 + K_2[\mathbf{n}\times(\nabla\times\mathbf{n})]^2 + K_3[\mathbf{n}\cdot(\nabla\times\mathbf{n})]^2,$$

due to splay, twist (K_2), and bend (K_3) deformations. These equations are already in rescaled form. We use the scaling introduced in [9] in which lengths, time, orientational elasticities, viscosities, dielectric permittivities, and voltages are measured in units of d/π (d: distance between the plates), director relaxation time τ_d, splay deformation constant K_1, $\gamma_1 = \tilde{\alpha}_3 - \tilde{\alpha}_2$, $\epsilon_0\epsilon_\perp$, and V_c, respectively, where

$$\tau_d = \frac{\gamma_1 d^2}{K_1\pi^2}, \quad V_c = \sqrt{\frac{K_1\pi^2}{\epsilon_0\epsilon_\perp}},$$

and $\epsilon_0\epsilon_\perp(\delta_{ij} + \varepsilon_a n_i n_j)$ and $\tilde{\alpha}_j (1\le j\le 6)$ are the unscaled dielectric permittivity tensor and the Leslie coefficients, respectively. The Prandtl-type number P_2 is the ratio $P_2 = \tau_{visc}/\tau_d$, where $\tau_{visc} = d^2\rho_m/\gamma_1$ is the viscous relaxation time and ρ_m is the mass density. Using the common planar alignment, the coordinate system is chosen such that $\mathbf{n}$=(1,0,0) at the upper and lower plates located at $z = \pm\pi/2$. We assume a constant external electric field in the z-direction and decompose the total field as usual into

$$\mathbf{E} = (\sqrt{2R}/\pi)\mathbf{e_3} - \nabla\phi,$$

where $\sqrt{2R}/\pi$ is the external field strength, and the internally generated field is derived from the potential ϕ. The tensors $\mathbf{d}$, $\mathbf{A}$, and $\mathbf{T}$ are, respectively, the projection tensor $d_{ij} = \delta_{ij} - n_i n_j$ that guarantees $|\mathbf{n}| = 1$, the shear flow tensor $A_{ij} = \frac{1}{2}(v_{i,j} + v_{j,i})$, and the viscous stress tensor

$$-T_{ij} = \alpha_1 n_i n_j n_k n_l A_{kl} + \alpha_2 n_j m_i + \alpha_3 n_i m_j + \alpha_4 A_{ij} + \alpha_5 n_j n_k A_{ki} + \alpha_6 n_i n_k A_{kj},$$

where $\mathbf{m} = \mathbf{d}(\lambda\mathbf{A}\mathbf{n} - \mathbf{h})$. The scaled Leslie coefficients $\alpha_1,\ldots,\alpha_6 (\alpha_j = \tilde{\alpha}_j/\gamma_1)$ and the Onsager coefficient λ in (1) satisfy the Onsager relations

$\alpha_1 + \alpha_3 = \alpha_6 - \alpha_5$, $\alpha_3 - \alpha_2 = 1$, and $\lambda = \alpha_5 + \alpha_6$. The tensor $\mathbf{\Pi}$ is the nonlinear Ericksen stress tensor with components $\mathbf{\Pi}_{ij} = (\partial f/\partial n_{k,j})\, n_{k,i}$.

The standard model for electroconvection [3–6] combines the continuum theory of Ericksen and Leslie with the quasistatic Maxwell equations under the assumption of an ohmic resistivity. In the weak electrolyte model (WEM) [2,8–10] the ohmic behaviour is replaced by the dynamics of two species of oppositely charged mobile ions. With this effect included, the local conductivity σ is not constant, but has to be treated as a further dynamic variable. In the approximation of a linear recombination term and zero diffusivity, the WEM consists of (1)–(3) and two balance equations for the charge density ρ and the local conductivity σ,

$$P_1(\partial_t + \mathbf{v}\cdot\nabla)\rho = -\nabla\cdot(\mu\mathbf{E}\sigma), \tag{4}$$

$$(\partial_t + \mathbf{v}\cdot\nabla)\sigma = -\alpha^2\pi^2\nabla\cdot(\mu\mathbf{E}\rho) - \frac{r}{2}(\sigma^2 - 1 - P_1\pi^2\alpha\rho^2), \tag{5}$$

together with Poisson's law,

$$\rho = \nabla\cdot(\epsilon\mathbf{E}),$$

where the rescaled dielectric tensor ϵ and conductivity tensor μ are given by $\epsilon_{ij} = \delta_{ij} + \epsilon_a n_i n_j$ and $\mu_{ij} = \delta_{ij} + \sigma_a n_i n_j$, respectively, and P_1 is the ratio of the charge relaxation time and the director relaxation time. Conductivities are measured in units of the equilibrium conductivity $\sigma_{eq} = (\mu^+ + \mu^-)en_0$, defined in terms of the mobilities $\mu^\pm$ and the equilibrium concentration n_0 of the ions. The parameters α, r are given by [9]

$$\alpha = \sqrt{\frac{\mu^+\mu^-\gamma_1\pi^2}{\sigma_{eq}d^2}}, \quad r = \frac{\tau_d}{\tau_{rec}},$$

with the recombination time τ_{rec}. Both of these parameters are Prandtl-type time scale ratios.

By virtue of Poisson's law, (1)–(5) are considered as a system of dynamical equations for $\mathbf{n}$, $\mathbf{v}$, p, ϕ, σ. These equations have to be supplemented by boundary conditions. We assume an infinitely extended NLC layer in both horizontal directions (x, y) and use 'rigid' vertical boundary conditions derived from ideal conducting plate conditions, rigid anchoring for the director, and finite viscosity [9],

$$\frac{\partial\sigma}{\partial z}, n_2, n_3, \phi, \mathbf{v} = 0 \quad \text{at } z = \pm\pi/2. \tag{6}$$

The rescaled WEM equations (1)–(6) depend on the basic bifurcation parameter R, four Prandtl-type time scale ratios P_1, P_2, α (mobility parameter)

and r (recombination parameter), and the following scaled material parameters: dielectric and conductivity coefficients ϵ_a and σ_a, elastic energy coefficients K_2, K_3, Leslie coefficients $\alpha_1,\ldots,\alpha_6$, and Onsager coefficient λ. Before rescaling there are five independent Leslie coefficients in terms of which all Onsager coefficients can be expressed. After rescaling there remain four independent ratios. We introduce the independent parameters (Miesowicz coefficients)

$$\eta_0 = \alpha_1 + \alpha_4 + \alpha_5 + \alpha_6, \quad \eta_1 = (-\alpha_2 + \alpha_4 + \alpha_5)/2,$$
$$\eta_2 = (\alpha_3 + \alpha_4 + \alpha_6)/2, \quad \eta_3 = \alpha_4/2,$$

and use the Onsager relations to express λ, $\alpha_1,\ldots,\alpha_6$ as

$$\lambda = \eta_1 - \eta_2, \quad \alpha_1 = \eta_0 - 2\eta_1 - 2\eta_2 + 2\eta_3 + 1, \quad \alpha_2 = -(1+\lambda)/2,$$
$$\alpha_3 = (1-\lambda)/2, \quad \alpha_4 = 2\eta_3, \quad \alpha_5 = 2\eta_1 - 2\eta_3 - (1+\lambda)/2,$$
$$\alpha_6 = 2\eta_2 - 2\eta_3 - (1-\lambda)/2.$$

Typically P_1, P_2 are very small compared to the order parameters [9,10], thus we take the limit $P_2 = 0$ (zero momentum diffusion time) and $P_1 = 0$ (zero charge relaxation time). In addition to the main bifurcation parameter R we are then left with ten independent parameters $\eta_0, \eta_1, \eta_2, \eta_3, \varepsilon_a, r, \sigma_a, \alpha, K_2, K_3$.

We note that the WEM equations are invariant under the reflection operations (fields which preserve their signs are suppressed)

$$(x, n_2, n_3, v_1) \to (-x, -n_2, -n_3, -v_1), \tag{7}$$
$$(y, n_2, v_2) \to (-y, -n_2, -v_2), \tag{8}$$
$$(z, n_3, v_3, \phi) \to (-z, -n_3, -v_3, -\phi), \tag{9}$$

and under arbitrary translations in x and y because we assume an infinitely extended layer, but there are no rotational symmetries due to the anisotropy of the system.

3. BIFURCATION ANALYSIS

We consider here the WEM equations (1)–(6) with $P_1 = P_2 = 0$. In this limit (2) and (4) do not depend on the time derivatives of v and ϕ, respectively, hence these variables play the role of 'slaved variables' leaving a dynamical system for three field variables $\mathbf{u} = (\sigma, n_2, n_3)$.

Linear Stability Analysis

The basic nonconvecting solution of (1)–(6) is given by $\sigma = 1$, $\mathbf{n} = (1,0,0)$, $\mathbf{v} = 0$, p = const, $\phi = 0$. The stability of this state is governed by linearized

equations for perturbational fields $\delta\sigma, \delta n_2, \delta n_3, \delta\phi, \delta v_j, \delta$p. Owing to the translation invariance w.r.t. (x, y), the perturbational fields are represented by horizontal Fourier modes,

$$(\delta\sigma, \delta n_2, \delta n_3, \delta\phi, \delta v_j, \delta p) = e^{i(px+qy)}(\mathbf{\Sigma}, N_2, N_3, \mathbf{\Phi}, V_j, \mathrm{P}),$$

where $\mathbf{\Sigma}, N_2$ etc. depend on (t, z, p, q) and the parameters. As usual the V_j and P are represented by poloidal and toroidal stream functions F and G leaving us with a system of linear equations for $(\mathbf{\Sigma}, N_2, N_3, \mathbf{\Phi}, F, G)$. Symbolically these equations can be written as

$$\partial_t \mathbf{U} = \mathbf{L_U}(\mathbf{U}, \mathbf{\Phi}, \mathbf{F}, p, q, R), \tag{10}$$

$$L_{\mathbf{\Phi}}(\mathbf{\Phi}, \mathbf{U}, p, q, R) = 0, \quad \mathbf{L_F}(\mathbf{F}, \mathbf{\Phi}, \mathrm{U}, p, q, R) = \mathbf{0}, \tag{11}$$

where $\mathbf{U} = (\mathbf{\Sigma}, N_2, N_3)$, $\mathbf{F} = (F, G)$, and $\mathbf{L_U}$, $L_{\mathbf{\Phi}}$, $\mathbf{L_F}$ are linear differential operators w.r.t. z that depend on (p, q, R) and the other parameters. The explicit form of these equations is summarized in the appendix (Eqs. (A.1)–(A.4) and (A.5)–(A.7)). Formally we view (10), (11) as a linear dynamical system for $\mathbf{U}$,

$$\partial_t \mathbf{U} = \mathbf{L}(\mathbf{U}, p, q, R), \tag{12}$$

where $\mathbf{L}$ is defined by substituting the solution $\mathbf{\Phi}[\mathbf{U}, p, q, R]$, $\mathbf{F}[\mathbf{U}, p, q, R]$ of (11) into $\mathbf{L_U}$. Note that this solution involves inversion of differential operators w.r.t. z and hence induces integral operators in $\mathbf{L}$.

Neutral stability of the basic state occurs on a neutral stability surface in (p, q, R) – space on which $\mathbf{L}$ has either a zero eigenvalue (stationary neutral stability surface) giving rise to a stationary bifurcation, or an imaginary eigenvalue (oscillatory neutral stability surface) giving rise to a Hopf bifurcation. We are interested in parameter regimes where the first instability when R increases is a Hopf bifurcation at $R = R_c$, with critical wave numbers (p_c, q_c), where (p_c, q_c, R_c) are the coordinates of the global R – minimum on the oscillatory neutral stability surface (ONSS).

Owing to the symmetry (9), $\mathbf{L}$ has odd and even invariant subspaces spanned by modes of the form $\mathbf{U}_m = (a_1 \sin(2m-1)z, a_2 \sin 2mz, a_3 \cos(2m-1)z), m \geq 1$, and $\mathbf{V}_m = (a_1 \cos 2mz, a_2 \cos(2m+1)z, a_3 \sin 2mz), m \geq 0$, respectively. For the parameter range considered here the instability occurs in the odd subspace. In this subspace $\mathbf{L}$ is represented by an infinite matrix $\mathbf{M}$ composed of 3×3 blocks $\mathbf{M}(m, n)$ defined by

$$M_{ij}(m, n) = (2/\pi) \int_{-\pi/2}^{\pi/2} \mathbf{L}(\mathbf{U}_{mi}) \cdot \mathbf{U}_{nj} dz, \quad 1 \leq i, j \leq 3, \tag{13}$$

where $\mathbf{U}_{mi}$ is the $\mathbf{U}_m$ mode with $a_j = \delta_{ij}$. To find these matrices we solve, for any $\mathbf{U}_{mi}$, the nonhomogeneous equations (11) subject to the boundary

conditions and evaluate the resulting integral (13) analytically. The solution of the $\mathbf{\Phi}$-equation is straightforward and preserves the chosen modes. In contrast, the solution of the $\mathbf{F}$-equation involves hyperbolic functions leading to a transcendental dependence of the M_{ij} on (p, q). We note that the matrix elements, when viewed as functions of (p, q), satisfy certain even/odd relations induced by the horizontal symmetries (7),(8).

For computing (p_c, q_c, R_c) numerically we used a $3N \times 3N$ truncation of $\mathbf{M}$ by restricting (m,n) to $1 \leq m, n \leq N$. We moved progressively to higher values on N using the previously computed values as starting values for the numerical search. For $N > 1$ the ONSS was computed with the aid of an augmented matrix, combined with a minimization procedure to find the critical values. For $N = 1$ the analytical conditions for an imaginary eigenvalue of a 3×3 matrix and for an R-minimum have been evaluated. Numerical convergence with an accuracy up to five significant figures usually was observed for $N \leq 9$.

Normal Form and Basic Wave Patterns

Two types of Hopf bifurcations have to be distinguished: ONSS-minima (p_c, q_c, R_c) with $q_c = 0$ and $q_c \neq 0$ (the case $p_c = 0$ does not occur). In our study we focus on the case $q_c \neq 0$. In this case the ONSS has four minima $(\pm p_c, \pm q_c, R_c)$ due to the two horizontal reflection symmetries. Accordingly, near onset, the bifurcating solutions are represented by four complex amplitudes $A_j (1 \leq j \leq 4)$ as a superposition of four oblique traveling rolls,

$$\mathbf{u}(t,x,y) = \epsilon \mathbf{U}_c(z) e^{i\omega_c t} \Big(A_1 e^{i(p_c x + q_c y)} + A_2 e^{i(-p_c x + q_c y)} + A_3 e^{i(-p_c x - q_c y)} + A_4 e^{i(p_c x - q_c y)} \Big) + \text{cc}, \quad (14)$$

where $\epsilon^2 \sim R - R_c$, $\mathbf{U}_c$ is the critical z-mode, ω_c is the critical frequency, and the amplitudes A_j are slowly varying. In this section we ignore spatial variation of the A_j (see Section 4), which corresponds to imposing periodic boundary conditions in (x, y) with spatial periods $(2\pi/p_c, 2\pi/q_c)$.

With spatial variation ignored, the A_j satisfy a system of normal form ODEs which is left invariant under three continuous symmetries ($t \to t + \tau, x \to x + \xi, y \to y + \eta$ in (15)), and two reflections symmetries ($x \to -x, y \to -y$ in (15)). Up to cubic order the ODE for A_1 is given by [16–18]

$$\frac{dA_1}{dT} = \left(a_0 + \sum_{j=1}^{4} a_j |A_j|^2 \right) A_1 + a_5 A_2 \bar{A}_3 A_4, \quad (15)$$

where $T = \epsilon^2 t$ and the a_j are complex coefficients derived from the original system, with $\epsilon^2 \text{Re}(a_0) \sim R - R_c$. The equations for A_2, A_3, A_4 follow from

(15) by applying the permutations (2,1,4,3), (3,1,4,2), (4,3,2,1) corresponding to the space reflections $x \to -x, (x,y) \to (-x,-y), y \to -y$. We have developed a code that allows us to compute the a_j in any N-mode approximation once (p_c, q_c, R_c) has been determined. Details of the procedure will be described elsewhere.

The normal form (15) has six basic periodic solutions corresponding to six distinct basic wave patterns shown by $\mathbf{u}(t,x,y)$ when represented by (15): traveling and standing rolls (*TW* and *SW*), two types of traveling rectangles (*TR*), standing rectangles (*SR*), and alternating waves (*AW*), which alternate periodically between differently oriented standing rolls, see Figure 1. Each of these waves can occur with different orientations, for

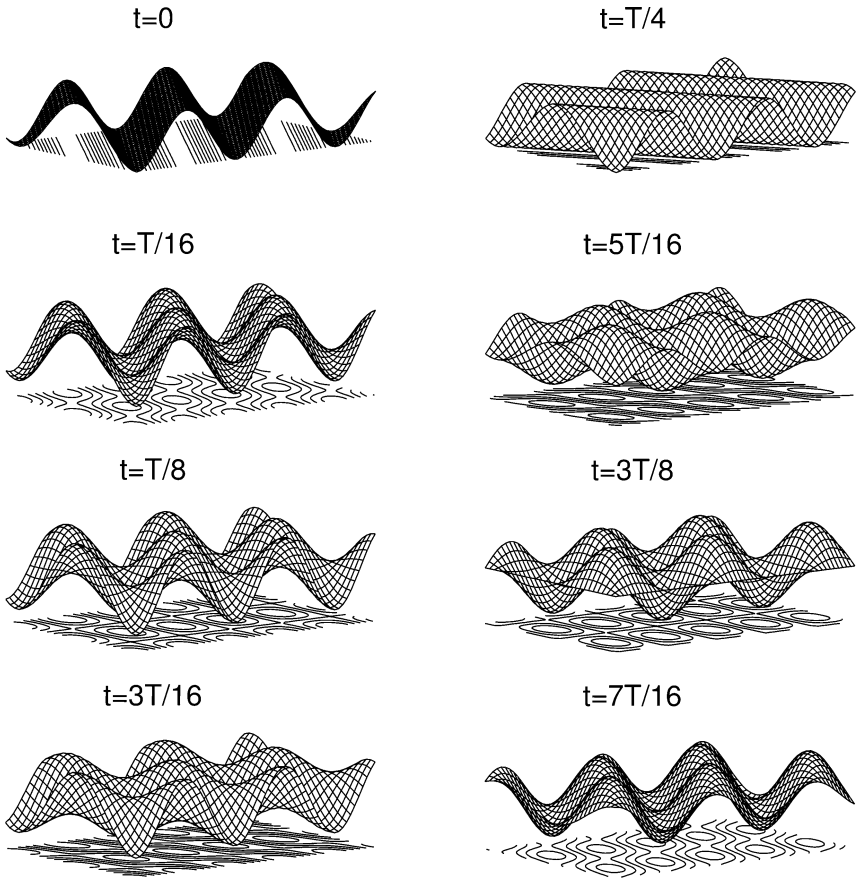

FIGURE 1 Snapshots of an alternating wave (amplitude versus x, y) during half of the period (T).

example a *TW* can propagate in any of the four directions $(\pm p_c, \pm q_c)$, and their stability is classified in terms of the nonlinear coefficients a_j (see [16–18]).

The dynamical repertoire of (15) is rich and not yet fully explored, but some facts are known. First, several (up to three) basic wave patterns can be simultaneously stable. Second, there are eight four-dimensional invariant subspaces and in one of them we can find quasiperiodic solutions. Third, several heteroclinic cycles connecting different basic periodic solutions can occur as attractors in certain parameter regimes.

Numerical Results

In our numerical investigation we varied K_2, K_3 in addition to the main bifurcation parameter R, and kept the remaining eight material parameters fixed at two different sets of values I and II as summarized in Table 1. The values of $\eta_0, \eta_1, \eta_2, \eta_3, \varepsilon_a, \sigma_a$ were chosen in accordance with measured values of the materials 152 [19] (set I) and MBBA I [20,21] (set II). The values of r and α have been chosen such that a Hopf bifurcation with $q_c \neq 0$ does indeed occur. For larger values of r or α the ONSS–minimum is always on the p-axis, or there is no Hopf bifurcation at all.

Of particular interest is the transition between $q_c = 0$ – and $q_c \neq 0$ – type Hopf bifurcations. This transition clearly marks a codimension two bifurcation at which an ONSS–minimum on the p axis degenerates in the y direction. If it exists and the remaining parameters are fixed, the codimension two points are located on a curve $K_3 = K_{3d}(K_2)$ in the (K_2, K_3) – plane. Above that curve the Hopf bifurcation occurs with $q_c = 0$, and below that curve q_c is nonzero. In Table 2 we present typical linear critical data computed for set I with $K_2 = 1.3$ and K_3 increasing towards the codimension two point. The table shows R_c, p_c, q_c together with the associated Hopf frequencies and the critical group velocities.

Our findings concerning the weakly nonlinear analysis are summarized in Figure 2 in the form of phase diagrams in the (K_2, K_3) – plane for the parameters sets I and II. In both diagrams the uppermost line connects the computed codimension two points. Below that line we find different

TABLE 1 Parameter Sets I and II

	η_0	η_1	η_2	η_3	ε_a	σ_a	r	α
I	0.8	0.9	0.05	0.1	0.02	0.8	0.8	0.3
II	09.8	1.23	0.23	0.38	−0.2	0.6	0.8	0.2

TABLE 2 Critical Values R_c, p_c, q_c, Associated Hopf Frequencies ω_c, and Critical Group Velocities v_{gx}, v_{gy} for Set I, with $K_2 = 1.3$ and K_3 Increasing Towards K_{3d} (Last Value)

K_3	R_c	p_c	q_c	ω_c	v_{gx}	v_{gy}
0.80	14.74	1.08	0.79	4.90	1.50	0.82
0.88	15.04	1.12	0.67	4.85	1.54	0.80
0.96	15.24	1.15	0.51	4.74	1.61	0.69
1.04	15.32	1.20	0.23	4.56	1.71	0.34
1.12	15.33	1.21	0.00	4.51	1.74	0.00

basic wave patterns occurring stably as solutions of (15) in different regions as marked in the diagrams. Note that for both parameter sets there is a certain range where *TW* and *AW* are simultaneously stable. Moreover, the parameter scans indicate the presence of a codimension three point that organizes transitions between *TW* and *AW* as well as the disappearance of stable basic patterns for small values of K_3. While in this range for set I the basic periodic solutions *TW* and *AW* are replaced by temporally quasiperiodic solutions (*QP*) residing in four dimensional invariant subspaces, the dynamics for small K_3 in case of set II has not yet been identified. We assume that here the attractors of (15) are heteroclinic cycles or higher dimensional tori. Examples of critical values (R_c,p_c,q_c), together with the associated Hopf frequencies and critical group velocities, are summarized in Table 2.

4. DISCUSSION

We have presented a numerical bifurcation analysis of the WEM equations (1)–(6) in the limit $P_1 = P_2 = 0$. Our main goal was to demonstrate the presence of a primary Hopf–type instability for which the patterns of the linearized system at threshold comprise four oblique traveling rolls with wave numbers $(\pm p_c, \pm q_c)$, and to analyze the stable convective waves predicted by this instability above threshold. The transition to an instability with a pair of counterpropagating waves (critical wave numbers $(\pm p_c, 0)$) was identified with a codimension two bifurcation leading to a separation boundary in the space of material parameters, which in this study was presented as a curve in the (K_2, K_3) – plane for fixed values of the other parameters. For the chosen parameter sets the predicted wave patterns below the separation curve turned out to be traveling rolls and alternating waves. For other choices of parameters we also found traveling and standing rectangles. The following remarks are in order:

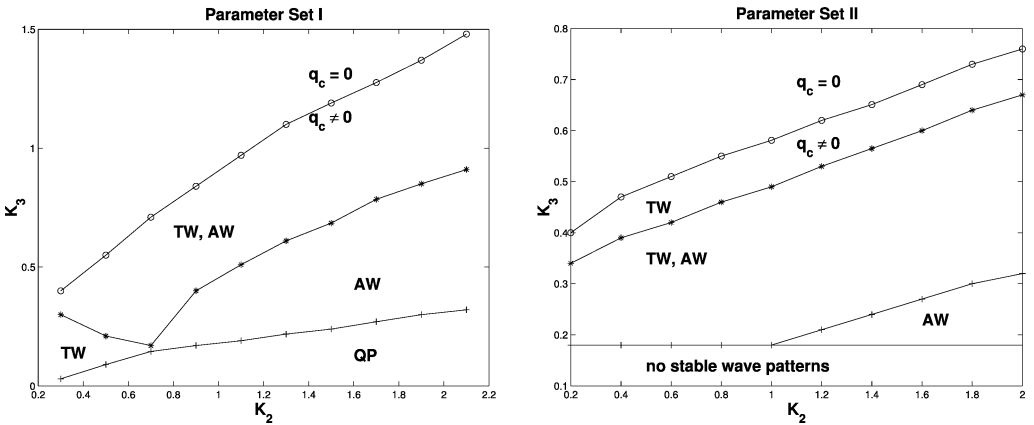

FIGURE 2 Stable wave patterns predicted by (15) for the parameter sets I and II.

1. The stability of the basic wave patterns has been determined solely on the basis of the ODE normal form (15), i.e. spatial variations of the amplitudes A_j are not taken into account. With spatial variations included, the A_j have to be considered as solutions of a system of envelope or modulation equations of the Ginzburg Landau type. If both critical group velocities v_{gx},v_{gy} are small (order ε), we are led to a system of coupled complex Ginzburg Landau equations. The equation for A_1 is given by

$$\partial_T A_1 - (v_{gx}\partial_X + v_{gy}\partial_Y)A_1 = \left(D + a_0 + \sum_{j=1}^{4} a_j |A_j|^2\right)A_1 + a_5 A_2 \bar{A}_3 A_4, \tag{16}$$

where $D = D_{20}\partial_X^2 + 2D_{11}\partial_{XY}^2 + D_{02}\partial_{YY}^2$, $(X, Y) = (\varepsilon x, \varepsilon y)$, and the D_{ij} are derived from the quadratic expansion of the ONSS and the frequency – wave number surface about (p_c, q_c). In some cases it is justified to set $A_2 = A_3 = 0$ (ignoring counterpropagating rolls). This leaves the system of two coupled complex Ginzburg Landau equations considered in [9,8], and excludes the possibility of alternating waves, standing rectangles, and one type of traveling rectangles.

On the other hand, if the critical group velocities are of order one, the two dimensional generalization of the globally coupled Ginzburg Landau equations given in [22] provide the correct description of the instability. In this case A_1, A_2, A_3, A_4 depend on $(\xi_+, \eta_+), (\xi_-, \eta_+), (\xi_-, \eta_-), (\xi_+, \eta_-)$, respectively, where $\xi_\pm = \varepsilon(x \pm v_{gx}t)$ and $\eta_\pm = \varepsilon(y \pm v_{gy}t)$ are slow wave variables. The resulting equation for A_1 is given by [18]

$$\begin{aligned}\partial_T A_1 = \Big\{ & D_1 + a_0 + a_1|A_1|^2 + a_2\langle|A_2(s,\eta_+)|^2\rangle \\ & + a_3\langle|A_3(\xi_+ + s, \eta_+ + s)|^2\rangle + a_4\langle|A_4(\xi_+, s)|^2\rangle\Big\}A_1 \\ & + a_5\langle A_2(\xi_+ + s, \eta_+)\bar{A}_3(\xi_+ + s, \eta_+ + s)A_4(\xi_+, \eta_+ + s)\rangle,\end{aligned} \tag{17}$$

where D_1 is another second order differential operator, and the brackets denote averages over s giving rise to global coupling terms. In general v_{gx}, v_{gy} are not small (see Table 2), and in this case equation (17) together with its permutations for A_2, A_3, A_4, are the correct envelope equations for a weakly nonlinear analysis. We are currently investigating Eckhaus stability boundaries for the wave patterns described in Section 3 on the basis of these equations.

2. In our numerical computation we avoided any special approximations and consistently checked numerical convergence. In particular exact

solutions of the nonhomogeneous velocity equations have been exploited to compute the matrix representation of the linearized system, in contrast to the commonly used approximation in terms of the lowest-order Chandrasekhar function. A comparison of the critical data obtained with our approach and the Chandrasekhar-mode approximation showed significant differences for some parameter values.

3. In this paper we considered a constant external electric field. If the external field is time periodic (ac field), the governing equations represent a parametrically forced spatial system. In future work we will extend our approach to include also this case. The linear stability analysis then requires the computation of Floquet exponents which is straightforward, though computationally more expensive. The ODE normal form (15) as well as the Ginzburg Landau systems (16),(17) are still valid generically (if there are no resonances).
4. In this investigation we varied (K_2, K_3) and kept the other material parameters fixed. Although the measured values $(K_2, K_3) \approx (0.6, 1.3)$ for 152 [19] and (0.7, 1.25) for MBBA I [20,21] at room temperature are above the condimension two separation curve, our numerical findings suggest that traveling rolls and alternating waves play a dominant role. In future work we will attempt to compute the separation boundary with (K_2, K_3) fixed as above, and α, r and the driving frequency of the external field varied.

APPENDIX

The linearized WEM equations depend on several anisotropic horizontal differential operators which become polynomials in (p, q) after Fourier transformation. To obtain a compact representation of these polynomials we introduce basic polynomials of the form $k_j^2 = c_p p^2 + c_q q^2 (0 \le j \le 12)$ in Table 3. The parameters a, b, c, η occurring in this table are defined by

$$a = \eta_0, \quad b = \frac{1}{4}[2(\eta_1 + \eta_2) - (\eta_1 - \eta_2)^2 - 1], \quad c = \eta_3, \eta = \eta_2 - \eta_1.$$

With this notation the linearized equations for $\sum, N_2, N_3$ take the form (prime denotes ∂_z)

$$\partial_t \mathbf{\Sigma} = -r\mathbf{\Sigma} - 2ip\alpha^2 \varepsilon_a R N_3' + \alpha^2 \pi \sqrt{2R}(\partial_z^2 - k_6^2)\mathbf{\Phi}', \tag{A.1}$$

$$\partial_t N_2 = 2(K_3 \partial_z^2 - k_2^2)N_2 - 2iq(K_3 - 1)N_3' - (i/2)L_2(\mathbf{V}), \tag{A.2}$$

$$\partial_t N_3 = 2(1 - K_3)iqN_2' + 2(\partial_z^2 + \varepsilon_a R - k_3^2)N_3 - \varepsilon_a \pi \sqrt{2R} ip\mathbf{\Phi} - (1/2)L_3(\mathbf{V}), \tag{A.3}$$

TABLE 3 Coefficients c_p, c_q in $k_j^2 = c_p p^2 + c_q q^2$

	k_0^2	k_1^2	k_2^2	k_3^2	k_4^2	k_5^2	k_6^2	k_7^2	k_8^2
c_p	c	b	K_2	K_2	$1-\eta$	$(1-\eta)K_3$	$1+\varepsilon_a$	$1+\sigma_a$	$1+(1+\eta)\dfrac{\varepsilon_a}{2}$
c_q	b	c	1	K_3	$1+\eta$	$1+\eta$	1	1	1

	k_9^2	k_{10}^2	k_{11}^2	k_{12}^2
c_p	$c-(1+\eta)\dfrac{c\varepsilon_a}{2}$	$(1+\eta)cK_2$ $+(1-\eta)$ $\times(c-bK_2-cK_3)$	$(1+\eta)K_2$ $+(1-\eta)(1-K_3)$	$(1+\eta)cK_2$ $+(1-\eta)c$
c_q	b	$(1+\eta)c-(1-\eta)bK_3$	$1+\eta$	$(1+\eta)c$ $+(1-\eta)bK_3$

where

$$L_2(\mathbf{V}) = (1+\eta)qV_1 - (1-\eta)pV_2, \quad L_3(\mathbf{V}) = (1+\eta)V_1' - (1-\eta)ipV_3,$$

and the V_j are expressed through F, G as

$$V_1 = iqG + cipF', \quad V_2 = -ipG + biqF', \quad V_3 = k_0^2 F. \tag{A.4}$$

Note that (A.4) differs slightly from the commonly used representation of velocities in terms of stream functions. The chosen form turns out to be particularly useful when solving the nonhomogeneous velocity equations.

The linearized equation for the potential reads

$$(\partial_z^2 - k_7^2)\Phi - (\sqrt{2R}/\pi)(\sigma_a ipN_3 + \Sigma') = 0, \tag{A.5}$$

and the equations for the stream functions are given by

$$(k_0^4 k_1^2 - B\partial_z^2 + bck_0^2\partial_z^4)F - sp^3 qG' + \pi\sqrt{2R}(k_9^2\partial_z^2 - k_8^2 k_0^2)\Phi + L_F(N_2, N_3) = 0, \tag{A.6}$$

$$(A - k_0^2\partial_z^2)G + sp^3 qF' + \varepsilon_a \pi\sqrt{R/2}(1+\eta)pq^{\Phi'} + L_G(N_2, N_3) = 0, \tag{A.7}$$

where $s = ac - 2bc - b^2 + c^2$, $A = bp^4 + (a - 2b + 2c)p^2q^2 + bq^4$, $B = c^2 (a - 2b + 2c)\, p^4 + b(b^2 + 3c^2)p^2q^2 + 2cb^2q^4$, and

$$\begin{aligned} L_F(N_2, N_3) &= pq\big\{[(1+\eta)c - (1-\eta)K_3 b]\partial_z^2 - k_{10}^2\big\}N_2' \\ &\quad - ip\big\{c(1+\eta)\partial_z^4 - [k_{12}^2 - (1+\eta)c\varepsilon_a R]\partial_z^2 \\ &\quad + [(1-\eta)k_3^2 + (1+\eta)\varepsilon_a R]k_0^2\big\}N_3, \\ L_G(N_2, N_3) &= (k_2^2 k_4^2 - k_5^2\partial_z^2)N_2 + iq[(1+\eta)(\partial_z^2 + \varepsilon_a R) - k_{11}^2]N_3'. \end{aligned}$$

REFERENCES

[1] Chandrasekhar, S. (1977). *Liquid crystals*, University Press: Cambridge.
[2] Pesch, W. & Behn, U. (1998). In: *Evolution of Spontaneous Structures in Dissipative Continuous Systems*, Busse, F. & Müller, S. (Eds.), Springer, pp. 335.
[3] Carr, E. F. (1969). *Mol. Cryst. Liq. Cryst.*, *7*, 253.
[4] Helfrich, W. (1969). *J. Chem. Phys.*, *51*, 4092.
[5] Penz, P. A. & Ford, G. W. (1972). *Phys. Rev. A*, *6*, 414.
[6] Zimmermann, W. & Kramer, L. (1985). *Phys. Rev. Lett.*, *55*, 402.
[7] Plaut, E. & Pesch, W. (1999). *Phys. Rew. E*, *59*, 2, 1747.
[8] Treiber, M. & Kramer, L. (1995). *Mol. Cryst. Liq. Cryst.*, *261*, 311.
[9] Treiber, M. PhD Thesis. (1996). *University of Bayreuth*.

[10] Treiber, M. & Kramer, L. (1998). *Phys. Rev. A*, *58*, 1973.
[11] Kai, S. & Hirakawa, K. (1978). *Progr. Theor. Phys. Suppl.*, *64*, 212.
[12] Rehberg, I., Rasenat, S., de la Torre Juarez, M., Schöpf, W., Hörner, F., Ahlers, G., & Brand, H. R. (1991). *Phys. Rev. Lett.*, *67*, 596.
[13] Denin, M., Cannell, D. S., & Ahlers, G. (1995). *Mol. Cryst. Liq. Cryst. Sci. Technol.*, Sect. A *261*, 377.
[14] Erickson, J. L. (1960). *Arch. Rat. Mech. Anal.*, *4*, 231.
[15] Leslie, F. M. (1966). *Quart. J. Mech. Appl. Math.*, *19*, 357.
[16] Silber, M., Riecke, H., & Kramer, L. (1992). *Physica D*, *61*, 260–78.
[17] Wegelin, M. PhD Thesis. (1993). *University of Tübigen*.
[18] Dangelmayr, G. & Wegelin, M. (1999). In: *Pattern Formation in Continuous and Coupled Systems*, Golubitsky, M., Luss, D., & Strogatz, S. (Eds.), IMA Vol. in *Math. and Appl.*, 115, Springer, 33–48.
[19] Denin, M., Ahlers, G., & Cannel, D. S. (1994). In: *Sptio-temporal Patterns in Non-equilibrium Complex Systems*, Cladis, P. & Palffy-Muhoray, P. (Eds.), Addison-Wesley, pp. 343.
[20] de Jeu, W. H., Classen, W. A. P., & Spruijt, A. M. J. (1976). *Mol. Cryst. Liq. Cryst.*, *37*, 369.
[21] Kneppe, H., Schneider, F., & Sharma, N. K. (1987). *J. Chem. Phys.*, *77*, 3203.
[22] Knobloch, E. & DeLuca, J. (1990). *Nonlinearity*, *2*, 975–980.